Luminescent Platinum(II) Terpyridyl Complexes: Effect of Counter Ions on Solvent-Induced Aggregation and Color Changes

Vivian Wing-Wah Yam,* Kenneth Hoi-Yiu Chan, Keith Man-Chung Wong,* and Nianyong Zhu[a]

Abstract: A series of platinum(II) terpyridyl complexes [Pt(tpy)(C≡C−C≡CH)]X, **1**-X (X = OTf^-; PF_6^-; ClO_4^-; BF_4^-; BPh_4^-); [Pt(tpy)(C≡CC_6H_5)]X, **2**-X (X = OTf^-; PF_6^-; ClO_4^-; BF_4^-); [Pt(tpy)(C≡C$C_6H_4OCH_3$-4)]OTf, **3**-OTf, and [Pt(4′-CH_3O-tpy)(C≡C-C_6H_5)]OTf, **4**-OTf (tpy = 2,2′:6′,2″-terpyridine, OTf = trifluoromethanesulfonate) were synthesized and their photophysical properties determined. Electronic absorption and emission studies showed the formation of a new band upon increasing the diethyl ether content in an acetonitrile/diethyl ether mixture. This was ascribed to the formation of complex aggregates, the solution color of which is dependent on the nature of the anions. This indicates that counter ions play an important role in governing the degree of aggregation and the extent of interactions within these aggregates. Addition of various anions to solutions of **1**-OTf and **1**-PF_6 produced anion-induced color changes upon solvent-induced aggregation, indicating that these complexes may serve as potential colorimetric anion probes.

Keywords: aggregation · alkynyl ligands · anion-induced color changes · photoluminescence · platinum

Introduction

The spectroscopic and photophysical behavior of square-planar platinum(II) complexes has been extensively studied in the past few decades, due to their intriguing spectroscopic and luminescence properties,[1–7] as well as their propensity to exhibit metal–metal interactions.[2–4] One class of such compounds is the platinum(II) terpyridyl complexes, the luminescence behavior of which has been reported.[3–7] Some of these complexes exhibit rich polymorphism in the solid state, with their luminescence properties highly dependent upon the temperature, type of counter ions, and solvents used for crystallization.[7] It has been suggested that the solid-state polymorphic behavior of these complexes and the variation in their luminescence colors are associated with the extent of metal–metal interactions and π–π stacking of the polypyridyl ligands.[4,7,8]

Recently, we reported the interesting solid-state polymorphism and "solvatochromism" of a platinum(II) alkynyl complex, [Pt(tpy)(C≡C−C≡CH)]OTf (tpy = 2,2′:6′,2″-terpyridine, OTf = trifluoromethanesulfonate).[4] Remarkable color change and emission enhancement were observed due to solvent-induced aggregation upon increasing the diethyl ether content in an acetonitrile/diethyl ether mixture.[4] Although the aggregation properties of platinum(II) terpyridyl complexes are known, most of the studies on metal–metal interactions and π–π stacking have focused on the structures and crystal packing of these complexes in the solid state, and the aggregate formation in solution has remained relatively less explored. As an extension of our previous studies, which showed that solvent-induced aggregation in solution,[4] as well as the nature of the counter ion in the solid state, may significantly influence the colors and spectroscopic properties of these compounds,[5] we investigated the effect of the nature of the counter ion on the solvent-induced aggregation properties of these platinum(II) terpyridyl alkynyl complexes. Herein we describe the preparation and photophysical studies of a series of platinum(II) terpyridyl alkynyl complexes with various counter anions: [Pt(tpy)(C≡C−C≡CH)]X, **1**-X (X = OTf^-; PF_6^-; ClO_4^-; BF_4^-; BPh_4^-); [Pt(tpy)(C≡CC_6H_5)]X, **2**-X (X = OTf^-; PF_6^-; ClO_4^-; BF_4^-); [Pt-

[a] Prof. Dr. V. W.-W. Yam, K. H.-Y. Chan, Dr. K. M.-C. Wong, Dr. N. Zhu
Centre for Carbon-Rich Molecular and Nano-Scale Metal-Based Materials Research
and Department of Chemistry, The University of Hong Kong
Pokfulam Road, Hong Kong (P. R. China)
Fax: (+852) 2857-1586
E-mail: wwyam@hku.hk

Supporting information for this article is available on the WWW under http://www.chemeurj.org/ or from the author.

 DOI: 10.1002/chem.200500106

(tpy)(C≡CC$_6$H$_4$OCH$_3$-4)]OTf, **3**-OTf, and Pt(4′-CH$_3$O-tpy)-(C≡CC$_6$H$_5$)]OTf **4**-OTf (tpy = 2,2′:6′,2″-terpyridine) (Figure 1). The effect of counter ions on the characteristics

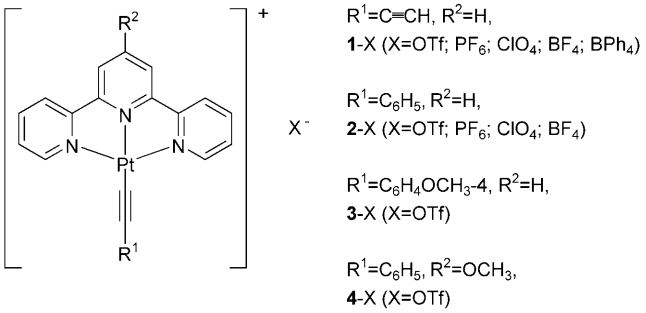

Figure 1. Schematic drawing of platinum(II) terpyridyl alkynyl complexes with various counter anions.

of the electronic absorption and emission spectra, in response to solvent-induced aggregation, is also reported. Some of these complexes have also been shown to exhibit anion-induced color changes and may serve as potential anion probes upon solvent-induced aggregate formation.

Results and Discussion

Syntheses and characterization: Complexes **1**-OTf, **2**-OTf, and **3**-OTf were synthesized as described previously.[4,5a] The corresponding derivatives of **1** and **2** containing different counter anions were prepared by the metathesis reaction in methanol, by using the respective ammonium or lithium salts. Interestingly, reaction of [Pt(4′-Cl-tpy)(MeCN)](OTf)$_2$] with phenylacetylene in refluxing methanol, in the presence of triethylamine, afforded **4**-OTf in satisfactory yield, in which the chloro group on terpyridine was replaced by the methoxy moiety. The identities of all complexes were fully established by performing ^{1}H NMR spectroscopy, IR spectroscopy, FAB mass spectrometry, and elemental analyses.

X-ray crystallography: Single crystals of **2**-ClO$_4$ (orange form) were obtained by the slow diffusion of diethyl ether vapor into an acetonitrile solution of **2**-ClO$_4$, and the crystal structure was determined by conducting X-ray crystallographic analysis. The molecular structure of the complex cation of **2**-ClO$_4$ is almost identical to that of **2**-PF$_6$,[5a] in which the platinum metal center adopts a slightly distorted square-planar geometry, coordinating with one terpyridyl ligand and one phenylacetylide ligand. Although the molecular structures of the complex cations of **2**-PF$_6$ and **2**-ClO$_4$ are very similar, their crystal colors (**2**-PF$_6$, dark brown; **2**-ClO$_4$, orange) are remarkably different. Such drastic color differences are ascribed to the differences in the crystal packing as a result of the influence of the counter anions. According to our previous studies,[5a] the dark brown form of **2**-PF$_6$ showed an extended linear array of molecules in the crystal packing, with short intermolecular Pt···Pt distances of between 3.36 and 3.38 Å. On the other hand, the crystal packing of **2**-ClO$_4$ revealed a head-to-tail stacking that formed a dimeric structure (Figure 2) with alternating

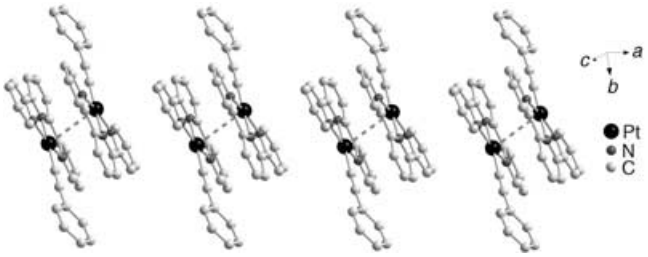

Figure 2. Crystal packing diagram of the complex cations of **2**-ClO$_4$.

"short" and "long" Pt···Pt distances of 3.452 and 7.727 Å, respectively. In addition, the molecules were arranged in a zigzag fashion with a Pt-Pt-Pt angle of 103.2°. The dimeric structure in the crystal packing of **2**-ClO$_4$ (orange form) suggests intermolecular Pt···Pt interactions that are confined mainly within the two metal centers. In contrast, a larger extent of metal–metal interactions is anticipated in the infinite linear-chain array of **2**-PF$_6$ (dark brown form), with nearly identical short Pt···Pt distances. Similar findings have also been reported in the crystal packing of the two crystal forms of **1**-OTf, the dark green form and the red form, which have been obtained by different recrystallization methods.[4] In general, crystal color that is characteristic of lower energy absorption would indicate the presence of shorter Pt···Pt distances or a larger extent of Pt···Pt interactions. Such polymorphism has been well studied in [Pt(bpy)Cl$_2$],[8a,c,d] which exhibits both red and yellow crystal forms, and in other platinum terpyridyl systems with variations in either the type of counter ion or the crystal forms.[7a]

Electrochemistry: The cyclic voltammograms of **1**-OTf, **2**-OTf, **3**-OTf, and **4**-OTf in acetonitrile (0.1 M nBu$_4$NPF$_6$) show two quasi-reversible reductions at around −0.96 and −1.47 V (vs saturated calomel electrode, SCE), and one irreversible oxidation at +1.02 to +1.64 V (vs SCE). The electrochemical data of selected complexes are summarized in Table 1. In view of the similar potentials for the reductions and oxidations in **2**-OTf and **2**-PF$_6$, it is suggested that there is no significant influence of counter anions on the electrochemical processes. In comparison to **2**-OTf, **4**-OTf, with an electron-rich, methoxy-substituted terpyridine ligand, showed more negative potentials for the reduction couples, whereas in the case of **3**-OTf, bearing a methoxy-substituent on the alkynyl group, a less positive potential for the oxidation wave was observed. With reference to previous studies on related platinum(II) complexes,[5a,d,6c] together with the trend observed in **2**-OTf, **3**-OTf, and **4**-OTf, the two reduction couples are assigned as the successive one-electron reduction of the terpyridine ligand, with some mixing of the

Table 1. Electrochemical data.

Complex	Oxidation E_{pa} [V] vs SCE	Reduction $E_{1/2}$ [V] vs SCE
1-OTf	+1.64	−0.96
		−1.43
2-OTf	+1.26	−1.06
		−1.40
2-PF_6[a]	+1.22	−0.97
		−1.46
3-OTf	+1.07	−1.05
		−1.42
3-PF_6[a]	+1.02	−1.05
		−1.46
4-OTf	+1.20	−1.17
		−1.47

[a] From reference [5a].

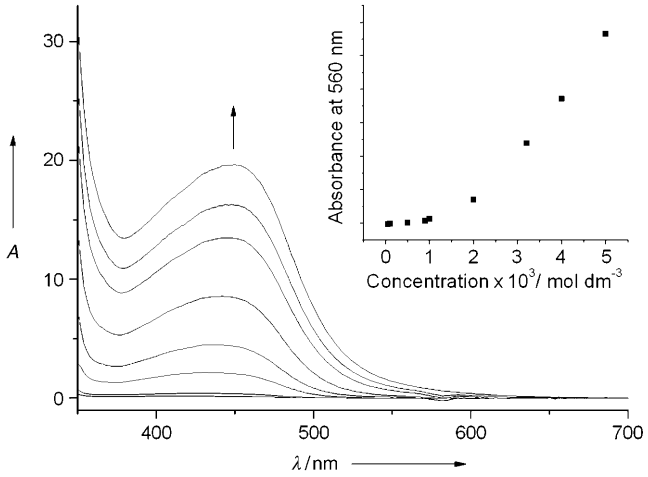

Figure 3. UV/Vis absorption spectral changes of **2**-BF_4 as concentration increases from 5×10^{-5} to 5×10^{-3} M. Inset: plot of absorbance at 560 nm as a function of concentration.

platinum(II) metal character. In contrast, the irreversible anodic waves are assigned as the metal-centered oxidation from Pt^{II} to Pt^{III}, probably mixed with some alkynyl ligand-centered oxidation. Such assignments are in line with observations that the reduction of **4**-OTf is more difficult relative to that of **2**-OTf, probably because of the presence of an electron-donating methoxy substituent on the terpyridine ligand, which would render the π*(tpy) orbital to a higher energy level. The increased ease of oxidation of **3**-OTf is ascribed to an increase in the energy of the dπ(Pt) orbital, due to its interaction with the higher-energy, electron-rich methoxy-substituted alkynyl ligand.

Electronic absorption and emission studies: Dissolution of complexes **1**–**4** in acetonitrile gave yellow to orange solutions with similar UV/Vis absorption patterns that included an intense absorption band at about 280–350 nm and a low-energy absorption band at around 405–477 nm at 298 K. The low-energy absorption band shows an energy trend of **3**-OTf (λ_{max} 477 nm) < **2**-OTf (434 nm) < **4**-OTf (423 nm). The photophysical data for these complexes are summarized in Table 2. With reference to previous spectroscopic work on platinum(II) terpyridyl alkynyl systems[3–7] and the observed energy trend, the higher-energy absorption band is assigned as intraligand (IL) [π→π*] transitions of the terpyridyl and alkynyl ligands. The lower-energy absorption band is assigned to a metal-to-ligand charge-transfer (MLCT) [dπ(Pt)→π*(tpy)] transition, with some mixing of an alkynyl-to-terpyridine ligand-to-ligand charge-transfer (LLCT) transition. This is in line with the better electron-donating ability of $C{\equiv}CC_6H_4OCH_3$-4 relative to $C{\equiv}CC_6H_5$, and the poorer π-accepting ability of 4′-CH_3O-tpy relative to tpy. Complex **2**-BF_4 was selected for the study of the concentration effect on electronic absorption spectroscopy, due to it having the best solubility in acetonitrile solution amongst the complexes studied. Different concentrations of **2**-BF_4 in acetonitrile were prepared, ranging from 5×10^{-3} to 5×10^{-5} M, and the UV/Vis absorption spectra of each concentration were recorded (Figure 3). At dilute concentrations (10^{-5} M), the lowest-energy absorption band was found to be at around 434 nm, and the growth of an absorption tail beyond 500 nm was observed for concentrated sample solutions. A plot of the absorbance of **2**-BF_4 at 560 nm versus concentration showed a nonlinear relationship that deviates from Beer's law. Such a deviation is suggestive of ground-state complex aggregation in acetonitrile at concentrations $\geq10^{-3}$ M.[3a,7a] The electronic absorption at $\lambda>500$ nm probably originates from metal–metal-to-ligand charge-transfer (MMLCT) transition as a result of the presence of intermolecular Pt···Pt contacts and π–π interactions in solutions of such high concentrations.

Because different colors of microcrystalline solid samples were obtained for different counter anions, solid-state absorption studies of each complex were performed, and the data are summarized in Table 2. The lowest-energy absorption band showed a red-shift in energy (ca. 488 nm–685 nm) relative to that in the solution state, which is probably due to the presence of Pt···Pt interactions and/or π–π stacking in the solid microcrystalline samples. A lower absorption energy was found in the solid-state absorption of **2**-PF_6 (642 nm) relative to that of **2**-ClO_4 (488 nm). This is in line with the stronger Pt···Pt and π–π stacking interactions in **2**-PF_6, as revealed by the extended linear array of closely spaced platinum centers in the crystal packing. The origin of these low-energy solid-state absorption bands is tentatively assigned as MMLCT transitions.

Our previous studies on **1**-OTf showed that a dramatic color change of the complex solution from yellow to blue occurred upon an increase in the diethyl ether composition in an acetonitrile/diethyl ether mixture.[4] Similar studies were performed on all other complexes, which showed (with the exception of **1**-BPh_4) similar changes in the UV/Vis absorption spectra. Remarkable color changes from yellow to blue, magenta, pink, and orange were also observed upon introduction of diethyl ether to the solutions of complexes **1**-OTf, **1**-PF_6, **1**-ClO_4, and **1**-BF_4, respectively. The spectroscopic data for these complexes are listed in Table 2. In general, the absorbance of the band at 370–470 nm decreases as

Table 2. Photophysical data for **1**–**4**.

Complex	Medium (T [K])	Appearance of sample[a]	Absorption data λ_{max}[b] [nm] (ε [$dm^3 mol^{-1} cm^{-1}$])	Emission λ_{em}[c] [nm] (τ_o [μs])	Φ_{lum}
1-OTf	CH_3CN (298)		238 (29950), 287 (21360), 312 (11130), 336 (13200), 406 (3940), [614]	670 (0.2), [785]	0.011
	solid (298)	dark green	685	–[e]	
	solid (77)	dark green		–[e]	
1-PF_6	CH_3CN (298)		238 (28420), 286 (20190), 312 (10570), 335 (12290), 405 (3840), [570]	670 (0.2), [726]	0.002
	solid (298)	dark red	596	800 (0.2)	
	solid (77)	dark red		–[e]	
1-ClO_4	CH_3CN (298)		239 (26390), 286 (19520), 312 (10400), 330 (11310), 405 (3540), [542]	670 (0.2), [738]	5×10^{-4}
	solid (298)	dark red	586	785 (0.2)	
	solid (77)	dark red		–[e]	
1-BF_4	CH_3CN (298)		238 (27080), 286 (19560), 311 (11150), 331 (12000), 405 (3610), [526]	670 (0.2), [735]	6×10^{-4}
	solid (298)	dark brown	556	770 (0.2)	
	solid (77)	dark brown		–[e]	
1-BPh_4	CH_3CN (298)		238 (25390), 288 (21080), 312 (11210), 336 (13320), 406 (4050), [–[d]]	–[f], [–[f]]	
	solid (298)	dark brown	–[d]	–[f]	
	solid (77)	dark brown		–[f]	
2-OTf	CH_3CN (298)		245 (36120), 262 (36980), 284 (23780), 312 (12820), 328 (12595), 342 (14250), 434 (4530), [630]	630 (0.5), [796]	0.012
	solid (298)	dark green	662	–[e]	
	solid (77)	dark green		–[e]	
2-PF_6	CH_3CN (298)		272 (33410), 286(23860), 312 (12450), 328 (12280), 342 (14440), 432 (4430), [650]	630 (0.5), [782]	0.012
	solid (298)	dark brown	642	–[e]	
	solid (77)	dark brown		–[e]	
2-ClO_4	CH_3CN (298)		245 (33620), 262 (34400), 283 (22160), 312 (11880), 328 (11670), 342 (13190), 434 (4180), [634]	630 (0.4), [760]	0.012
	solid (298)	orange	488	608 (<0.1)	
	solid (77)	orange		640 (0.7)	
2-BF_4	CH_3CN (298)		245 (34480), 262 (35600), 283 (22950), 312 (12490), 328 (12240), 342 (13830), 434 (4380), [724]	630 (0.5), [–[e]]	0.012
	solid (298)	dark brown	608	787 (<0.1)	
	solid (77)	dark brown		824 (0.7)	
3-OTf	CH_3CN (298)		268 (39570), 307 (13110), 329 (12640), 344 (12160), 418 sh (3240), 477 (4560), [736]	–[f], [–[e]]	
	solid (298)	dark red	610	784 (<0.1)	
	solid (77)	dark red		813 (0.9)	
4-OTf	CH_3CN (298)		247 (40370), 260 (40060), 283 (33360), 304 (13920), 319 (12750), 337 (13030), 423 (5140), [624]	607 (0.5), [769]	0.025
	solid (298)	dark red	674	–[e]	
	solid (77)	dark red		–[e]	

[a] Appearance of the microcrystalline samples. [b] Values in square parentheses refer to absorption bands formed due to solvent-induced aggregation. [c] Values in square parentheses refer to emission bands formed upon excitation at the isosbestic points of the UV/Vis spectral traces in solution. [d] MMLCT absorption band not observed. [e] Emission maximum (>850 nm) not located because it is beyond the range of the detector. [f] Non-emissive.

a new absorption band at 526–736 nm grows, with well-defined isosbestic points for complexes having OTf^- and BF_4^- as the counter ion, upon increasing the diethyl ether content. The proportions of diethyl ether required to induce formation of the new absorption band and to reach saturation are about 65–70 and 85–90%, respectively, depending on the nature of the complex cations and their counter anions. Figure 4 depicts the representative changes in the electronic absorption spectra of **1**-BF_4 and **2**-PF_6 in various compositions of an acetonitrile/diethyl ether mixture. The dramatic color changes are ascribed to ground-state oligomerization or aggregate formation of the complex in solution as a result of reduced solvation, arising from an increase in the diethyl ether content. The origin of the new absorption bands that impart the dramatic color change is tentatively assigned as MMLCT transition, due to the presence of Pt···Pt interactions and/or π–π stacking arising from the aggregate formation or oligomerization. Similar to the MLCT absorptions, the low-energy MMLCT absorptions also show energy trends, **3**-OTf < **2**-OTf and **2**-OTf < **4**-OTf, which follows the degree of electron-richness of the substituent on the alkynyl ligand and the π-accepting ability of the terpyridine group. Interestingly, unlike the MLCT bands in which the λ_{max} values for the same complex, but with different anions, are almost identical, the absorption energies of the MMLCT bands, and hence the associated colors, would vary

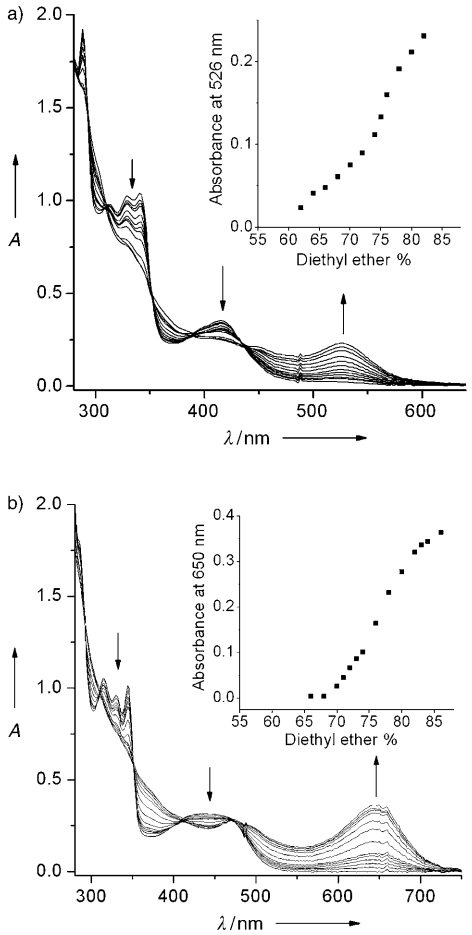

Figure 4. Changes in UV/Vis absorption of a) **1**-BF_4 and b) **2**-PF_6 in acetonitrile (concentration $=7\times10^{-5}$ M) as the percentage of diethyl ether increases. Insets: plots of absorbance as a function of diethyl ether composition.

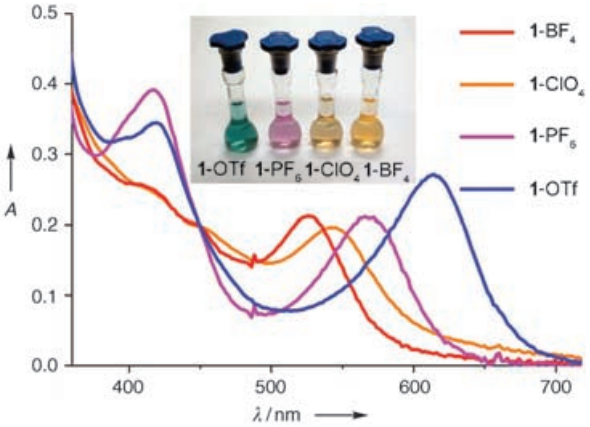

Figure 5. UV/Vis absorption spectra of **1**-OTf, **1**-PF_6, **1**-ClO_4, and **1**-BF_4 in an acetonitrile/diethyl ether mixture (concentration $=7\times10^{-5}$ M) at room temperature. Inset: Photograph of the corresponding solutions displaying the remarkable color differences upon solvent-induced aggregation. The diethyl ether content from left to right: 86%, 86%, 82%, 82%.

with the nature of the counter anions involved. Upon solvent-induced aggregation, the solution colors change from yellow to blue in **1**-OTf, to magenta in **1**-PF_6, to pink in **1**-ClO_4, and to orange in **1**-BF_4. Figure 5 illustrates the color changes of these four complexes in an acetonitrile/diethyl ether mixture, and their corresponding electronic absorption spectra. A strong dependence of the color of the aggregates of **1** on the nature of the counter anions is observed. Similarly, a change in the MMLCT absorption energies was observed in **2**, although these are less readily detected as a visual color change in response to a change in the nature of the counter ions. To the best of our knowledge, the present work represents the first study of its kind on the effect of counter ion on the aggregation or oligomerization properties of molecules in the solution state. We suggest that the variations in the absorption energies of the new bands as a function of counter ions are due to the different degrees of Pt···Pt and π–π interactions, depending on the Pt···Pt distance and the π–π stacking, as well as the degree of aggregation or oligomerization. The size and shape of the counter anions probably play crucial roles in governing the degree of the metal–metal and π–π interactions and oligomerization. The less-sensitive shifts in the MMLCT energies in the series of complexes **2** relative to those of **1** may be ascribed to the larger steric bulk of the $C{\equiv}CC_6H_5$ group relative to $C{\equiv}C{-}C{\equiv}CH$, which reduces the effect of the counter ions on the packing of the aggregates or oligomers. In addition, the possibility of interactions or hydrogen bonding between the acetylenic proton and the anions should also not be excluded in view of the possible complexation between HX (X = Br, Cl, F) and acetylene molecules predicted by theoretical calculations, and the observation of interactions between anions and protons attached to unsaturated carbon backbones.[9] The lack of solvent-induced aggregation in **1**-BPh_4, in which a larger size and noncoordinating BPh_4 anion was employed, further supports this hypothesis. In general, assuming that the aggregates or oligomers contain the same number of repeating units, a lower MMLCT energy would imply the presence of a stronger Pt···Pt and π–π interaction. Notably, although the molecular structures and crystal packings of the related platinum(II) terpyridyl complexes [Pt(tpy)Cl]X (X = OTf^-, PF_6^-, ClO_4^-, and Cl^-) have been revealed by X-ray crystallography, no simple systematic correlation between the nature of anions and their solid-state colors could be made.[7a] Aggregate solutions of complexes **2**–**4** were not as stable as solutions of **1**; precipitates were formed upon prolonged standing, probably due to the poorer solubility of **2**–**4** in the presence of the aryl alkynyl moiety.

In acetonitrile solution at 298 K and upon excitation at $\lambda > 400$ nm, **1** and **2** (3.5×10^{-5} M), with the exception of **1**-BPh_4, exhibit emission bands at around 670 and 630 nm, respectively (Table 2). These probably originate from an excited state of predominantly ^{3}MLCT character. The blue-shift in both the absorption and emission bands of **4**-OTf relative to those of **2**-OTf is consistent with an assignment of predominantly MLCT character, as the electron-donating methoxy substituent on the terpyridyl ligand would render the

π*(tpy) orbital to a higher energy level, and hence give rise to a higher MLCT transition energy. Because the electronic absorption spectrum of **2**-BF_4 in acetonitrile showed a growth in the absorption tail upon increasing the concentration beyond 10^{-3} M, corresponding studies of this concentration effect on the emission properties were also performed within the concentration range 10^{-6}–10^{-3} M. At concentrations higher than 10^{-3} M, a new emission band was formed with λ_{em} beyond 850 nm. Based on the UV/Vis absorption studies, together with the observation that the corresponding excitation spectra monitored at 830 nm also showed a tail at about 650 nm, the new emission band was suggested tentatively to be derived from the ^{3}MMLCT excited state resulting from aggregate formation.

The solid-state emission properties of **1**-X were studied. Although the emission of **1**-OTf had a band maximum beyond the range of the instrument response (>850 nm), **1**-PF_6, **1**-ClO_4, and **1**-BF_4 displayed a weak emission band at around 770–800 nm at 298 K, with a shift in the emission energies to the red at 77 K upon excitation at $\lambda > 550$ nm. Complex **1**-BPh_4 was non-emissive at both temperatures. In contrast, complexes **2**–**4** showed intense emission bands in the solid state, with the emission maximum of **2**-OTf occurring at wavelengths >850 nm. The solid-state emission properties appeared to be closely related to the solid-state absorption properties, with the solid-state emission energy trend of **2**-X closely aligned to that of the absorption energy trend. Similarly, the low-energy emissions beyond 680 nm in the solid state probably originate from triplet states of MMLCT character, associated with the presence of Pt···Pt interactions.

Apart from the drastic solution color changes resulting from the formation of a new band in the electronic absorption spectra of **1**–**4** (except **1**-BPh_4) with increasing diethyl ether content, a new intense emission band with μ_{em} beyond 700 nm appeared and grew in intensity with a concomitant diminishment of the ^{3}MLCT emission band at about 600–670 nm in solution upon excitation at the isosbestic points of the UV/Vis spectral traces. The emission changes of **1**-BF_4 and **2**-PF_6 in different compositions of acetonitrile/diethyl ether mixtures are shown in Figure 6, and their excitation bands were observed at 530 and 650 nm, respectively, upon monitoring at the near infra-red (NIR) emission. The new absorption bands in the electronic absorption spectra, and the excitation bands in the excitation spectra monitored at the corresponding new intense emission bands beyond 700 nm, closely resemble each other. The close resemblance of the new absorption bands in the electronic absorption spectra and the excitation bands in the excitation spectra monitored at the corresponding new intense emission bands beyond 700 nm, together with the consistency of emission intensity changes with absorbance changes as a function of diethyl ether content (Figure 4 inset and Figure 6 inset), suggested that they are derived from the same origin. Accordingly, the new emission bands of **1**–**4** are probably derived from states of ^{3}MMLCT character, resulting from solvent-induced aggregate formation. The occurrence of a higher-energy emission in **4**-OTf relative to that in **2**-OTf is also consistent with the ^{3}MMLCT assignment. In accordance with the observation of electronic absorption spectral changes, the emission energies of the new band of **1**-OTf, **1**-PF_6, **1**-ClO_4, and **1**-BF_4 upon formation of aggregates are dependent on the nature of the associated counter anions (Table 2).

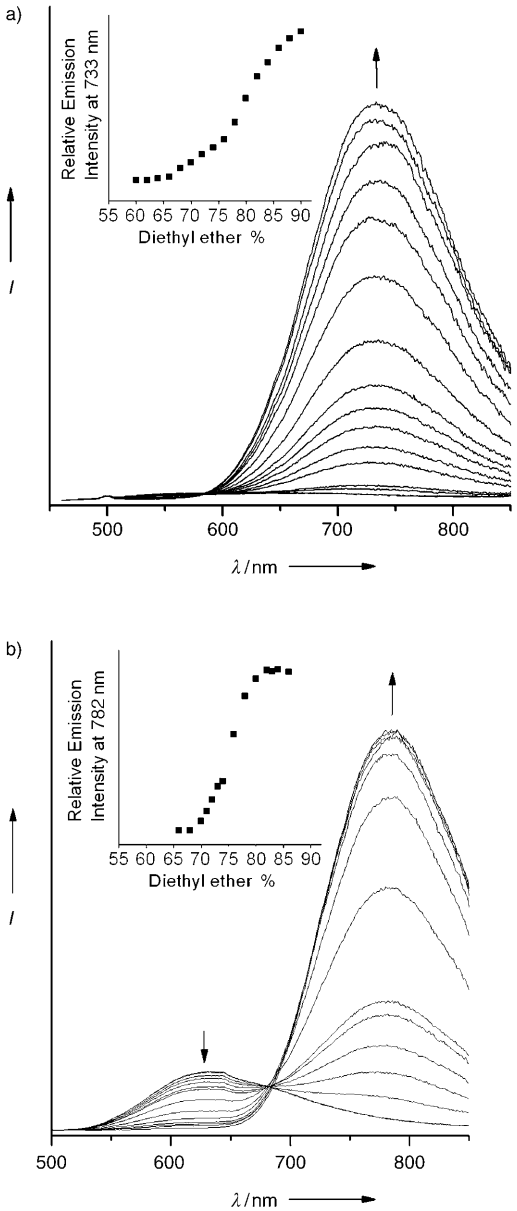

Figure 6. Corrected emission spectral changes of a) **1**-BF_4 and b) **2**-PF_6 in acetonitrile (concentration $= 7 \times 10^{-5}$ M) as the percentage of diethyl ether increases. Insets: plots of corrected emission intensity versus diethyl ether composition.

Anion-induced color changes: Addition of 1.5 M equivalent or more of NH_4PF_6, $LiClO_4$, and NH_4BF_4 to an acetonitrile solution of **1**-OTf (4×10^{-5} M), followed by the subsequent addition of diethyl ether to induce aggregate formation,

gave rise to a clear color change from blue to magenta, pink, and orange, respectively. Similarly, addition of AgOTf and NH_4BF_4 to an acetonitrile solution of **1**-PF_6, followed by addition of diethyl ether, converted the aggregate solution from magenta to blue and orange, respectively. These findings demonstrate that these complexes show anion-induced color changes and may have potential as colorimetric anion probes upon solvent-induced aggregation.

Conclusion

Solvent-induced aggregation of platinum(II) terpyridyl alkynyl complexes gave rise to drastic color changes and emission enhancement in the NIR region. Counter ions were shown to play an important role in governing the degree of aggregation and the extent of interactions within these aggregates. Such dependence of aggregate colors on the nature of the anions may be explored for applications in the development of colorimetric anion probes.

Experimental Section

Materials and reagents: Dichloro(1,5-cyclooctadiene)platinum(II), 2,2′:6′,2″-terpyridine, ammonium hexafluorophosphate and ammonium tetrafluoroborate were obtained from Strem Chemicals. Lithium perchlorate and 4′-chloro-2,2′:6′,2″-terpyridine (4′-Cl-tpy) were purchased from Acros Organics. Phenylacetylene and 1,4-bis(trimethylsilyl)-1,3-butadiyne were obtained from Aldrich Chemical and GFS Chemicals, respectively. (4-Methoxyphenyl)acetylene was purchased from Maybridge Chemical, [Pt(tpy)(MeCN)](OTf)$_2$ and [Pt(4′-Cl-tpy)(MeCN)](OTf)$_2$ were synthesized by modification of the literature method.[7b] All solvents were purified and distilled before use by using standard procedures. All other reagents were of analytical grade and were used as received.

Safety note: Perchlorate salts of metal complexes with organic ligands and $LiClO_4$/MeOH are potentially explosive and should be handled with care.

Physical measurements and instrumentation: ^{1}H NMR spectra were recorded by using a Bruker DPX 300 (300 MHz) or Bruker DPX 400 (400 MHz) Fourier transform NMR spectrometer, with chemical shifts reported relative to tetramethylsilane (Me_4Si). Positive-ion FAB mass spectra were recorded by using a Finnigan MAT95 mass spectrometer. IR spectra were obtained as Nujol mulls on KBr disks and a Bio-Rad FTS-7 Fourier transform infrared spectrophotometer (4000–400 cm^{-1}). Elemental analyses were performed by using a Carlo Erba 1106 elemental analyzer at the Institute of Chemistry, Chinese Academy of Sciences. The electronic absorption spectra were obtained by using a Hewlett–Packard 8452 A diode array spectrophotometer and a 1 cm or 1 mm path-length quartz cuvette. The concentrations of solution samples for electronic absorption measurements were typically in the range of 4×10^{-4} to 8×10^{-5} M. Solid samples were freshly recrystallized and the microcrystalline samples were sonicated in a beaker containing diethyl ether solution for five minutes. The finely dispersed sample suspensions were directly used for solid-state electronic absorption measurements. Steady-state excitation and emission spectra at room temperature and at 77 K were recorded by using a Spex Fluorolog-2 Model F111 fluorescence spetrofluorometer. Solid-state photophysical studies were carried out with solid samples contained in a quartz tube inside a quartz-walled Dewar flask, and all solid samples were freshly recrystallized. Measurements of the solid-state samples at 77 K were similarly recorded by using liquid nitrogen filled in the optical Dewar flask. All solutions for photophysical studies, with the exception of solution samples for solvent-induced aggregation studies, were degassed on a high-vacuum line in a two-compartment cell consisting of a 10 mL Pyrex bulb and a 1 cm path-length quartz cuvette, and sealed from the atmosphere by using a Bibby Rotaflo HP6 Telflon stopper. The solutions were rigorously degassed with at least four successive freeze-pump-thaw cycles. Luminescence quantum yields of **1**-OTf, **1**-PF_6, **1**-ClO_4, and **1**-BF_4 were measured by the optical dilute method,[10a] using a degassed aqueous solution of [Ru(bpy)$_3$]Cl$_2$ ($\Phi=0.042$, excitation wavelength at 455 nm)[10b] as the standard, and yields of **2**-OTf, **2**-PF_6, **2**-ClO_4, **2**-BF_4, and **4**-OTf were measured by using a degassed acetonitrile solution of [Ru(bpy)$_3$]Cl$_2$ ($\Phi=0.062$, excitation wavelength at 436 nm)[10c] as the standard. Emission lifetime measurements (concentration $=3.5\times10^{-5}$ M) were performed by using a conventional laser system. The excitation source used was a 355 nm output (third harmonic) from a Spectra-Physics Quanta-Ray Q-switched GCR-150–10 pulsed Nd-YAG laser. Luminescence decay signals were detected by using a Hamamatsu R928 PMT and recorded on a Tektronix Model TDS-620 A (500 MHz, 2 GS s^{-1}) digital oscilloscope, then analyzed by using a program for exponential fits. Cyclic voltammetric measurements were performed by using a CH Instruments model CHI 750 A Electrochemical Analyser. Electrochemical measurements were performed by using acetonitrile solutions with 0.1 M nBu_4NPF_6 (TBAH) as the supporting electrolyte at room temperature. The reference electrode was a $Ag/AgNO_3$ (0.1 M in acetonitrile) electrode and the working electrode was a glassy carbon electrode (Model No. CHI 104, CH Instruments) with a platinum wire as the counter electrode. The working electrode surface was first polished with 1 μm alumina slurry (CH Instruments) on a microcloth (Buehler). It was then rinsed with ultrapure, deionized water and sonicated in a beaker containing ultrapure water for five minutes. The polishing and sonicating steps were repeated twice and the working electrode was finally rinsed under a stream of ultrapure, deionized water. The ferrocenium/ferrocene couple ($FeCp_2^{+/0}$) was used as the internal reference. All solutions for electrochemical studies were deaerated with prepurified argon gas prior to taking measurements.

Crystal structure determination: Single crystals of **2**-ClO_4 were obtained by the slow diffusion of diethyl ether vapor into an acetonitrile solution of the complex. A crystal of dimensions $0.4\times0.15\times0.1$ mm mounted in a glass capillary was used for data collection at −20 °C by using a MAR diffractometer with a 300 mm image plate detector and graphite monochromatized $Mo_{K\alpha}$ radiation ($\lambda=0.71073$ Å). Data was collected by using a 2° oscillation step of ϕ, 10 min exposure time, and scanner distance at 120 mm. 100 images were collected. The images were interpreted and intensities integrated by using program DENZO.[11a] The structure was solved by direct methods employing the SHELXS-97 program.[11b] Pt, Cl, and most non-hydrogen atoms were located according to direct methods. The positions of the other non-hydrogen atoms were found after successful refinement by full-matrix least-squares analysis using program SHELXL-97.[11c] According to this program,[11c] all 3518 independent reflections (R_{int}[11d] equal to 0.0372, 3085 reflections larger than $4\sigma(F_o)$) from a total of 14865 reflections participated in the full-matrix least-squares refinement against F^2. These reflections were in the range $-9\le h\le9$, $-21\le k\le21$, $-15\le l\le15$, with $2\theta_{max}$ equal to 50.9°. One crystallographic asymmetric unit consists of one formula unit, including one perchlorate anion. Convergence ($(\Delta/\sigma)_{max}=0.001$, average 0.001) for 289 variable parameters by full-matrix least-squares refinement on F^2 reaches to $R_1=0.0264$ and $wR_2=0.0751$, with a goodness-of-fit of 1.107. The final difference Fourier map shows maximum rest peaks and holes of 0.870 and −1.708 e Å^{-3}, respectively. The perspective drawing of the complex cation of **2**-ClO_4 and text describing details of crystal and structure refinement data are given as Supporting Information. CCDC-261575 (**2**-ClO_4) contains the supplementary crystallographic data for this paper. These data can be obtained free of charge from the Cambridge Crystallographic Data Center via www.ccdc.ac.uk/data_request/cif.

Syntheses of platinum(II) complexes [Pt(tpy)(C≡C−C≡CH)]OTf (1-OTf): The complex was synthesized as described previously.[4] 1,4-Bis(trimethylsilyl)-1,3-butadiyne (304 mg, 1.56 mmol) and potassium fluoride (136 mg, 2.35 mmol) were placed in a round-bottomed flask and methanol (50 mL) was added. The resultant solution was heated to 50 °C for 30 min. Complex [Pt(tpy)(MeCN)](OTf)$_2$ (300 mg, 0.39 mmol) was added to the reaction mixture, and the orange solution was stirred at 50 °C for

5 h. The solvent was then evaporated under reduced pressure. The residue was washed with a small amount of methanol and was then dissolved in acetonitrile. Subsequent recrystallization by diffusion of diethyl ether vapor into an acetonitrile solution of the product gave **1**-OTf as dark green crystals. Yield: 150.2 mg (62%). ^{1}H NMR (300 MHz, CD_3CN, 298 K): $\delta = 8.70$ (d, $J = 5.6$ Hz, 2H; tpy), 8.40 (t, $J = 8.1$ Hz, 1H; tpy), 8.32–8.18 (m, 6H; tpy), 7.64 (dt, $J = 1.5$, 5.6 Hz, 2H; tpy), 2.26 ppm (s, 1H; acetylenic H); IR (Nujol): $\tilde{\nu} = 3480$(br) ν(O-H), 2156(m), 2010(w) ν(C≡C), 1150(s) cm^{-1} ν(S=O); positive-ion FAB-MS: *m*/*z*: 1103 $[2M-\text{OTf}]^+$, 477 $[M-\text{OTf}]^+$; elemental analysis calcd (%) for $C_{20}H_{12}N_3F_3SO_3Pt\cdot H_2O$: C 37.34, H 2.17, N 6.52; found: C 37.42, H 1.86, N 6.68.

[Pt(tpy)(C≡CC$_6$H$_5$)]OTf (2-OTf): The complex was prepared according to modification of a method previously reported by us.[5a] Sodium hydroxide (42 mg, 1.05 mmol) was added to a stirred solution of phenylacetylene (80 mg, 0.78 mmol) in methanol (25 mL). The resultant solution was stirred at room temperature for 30 min. Complex $[Pt(tpy)(MeCN)](OTf)_2$ (543 mg, 0.71 mmol) was added to the reaction mixture, which immediately became a deep red solution that was then stirred for 12 h at room temperature. The mixture was filtered and the filtrate was evaporated under reduced pressure. The product was dissolved in acetonitrile and filtered. Subsequent recrystallization by diffusion of diethyl ether vapor into an acetonitrile solution of the product gave **2**-OTf as dark green crystals. Yield: 351.4 mg (73%). ^{1}H NMR (400 MHz, CD_3CN, 298 K): $\delta =$ 9.10 (d, $J = 6.1$ Hz, 2H; tpy), 8.37–8.17 (m, 7H; tpy), 7.73 (t, $J = 6.1$ Hz, 2H; tpy), 7.48–7.29 ppm (m, 5H; C_6H_5); IR (Nujol): $\tilde{\nu} = 2122$(m) ν(C≡C), 1150(s) cm^{-1} ν(S=O); positive-ion FAB-MS: *m*/*z*: 529 $[M-\text{OTf}]^+$; elemental analysis calcd (%) for $C_{24}H_{16}F_3N_3SO_3Pt$: C 42.48, H 2.38, N 6.19; found: C 42.47, H 2.44, N 6.19.

[Pt(tpy)(C≡CC$_6$H$_4$-4-OCH$_3$)]OTf (3-OTf): The procedure was similar to that for **2**-OTf, except that (4-methoxyphenyl)acetylene (103 mg, 0.78 mmol) was used in place of phenylacetylene. Yield: 402.1 mg (80%). ^{1}H NMR (400 MHz, CD_3CN, 298 K): $\delta = 8.81$ (d, $J = 6.5$ Hz, 2H; tpy), 8.25–8.17 (m, 3H; tpy), 8.05–7.99 (m, 4H; tpy) 7.60 (t, $J = 6.6$ Hz, 2H; tpy), 7.26 (d, $J = 8.8$ Hz, 2H; Ph), 6.92 (d, $J = 8.8$ Hz, 2H; C_6H_4), 3.86 ppm (s, 3H; acetylenic H); IR (Nujol): $\tilde{\nu} = 3494$(br) ν(O-H), 2120(w) ν(C≡C), 1169(s) cm^{-1} ν(S=O); positive-ion FAB-MS: *m*/*z*: 559 $[M-\text{OTf}]^+$; elemental analysis calcd (%) for $C_{25}H_{18}N_3F_3O_4SPt\cdot 1.5H_2O$: C 40.82, H 2.88, N 5.71; found: C 40.75, H 2.80, N 5.83.

[Pt(4′-CH$_3$O-tpy)(C≡CC$_6$H$_5$)]OTf (4-OTf): The procedure was similar to that for **2**-OTf, except that $[Pt(4'\text{-Cl-tpy})(MeCN)](OTf)_2$ (568 mg, 0.71 mmol) was used in place of $[Pt(tpy)(MeCN)](OTf)_2$, and the reaction was heated to reflux in methanol for 12 h. Yield: 326.7 mg (65%). ^{1}H NMR (300 MHz, CD_3CN, 298 K): $\delta = 9.09$ (d, $J = 5.40$ Hz, 2H; tpy), 8.31–8.19 (m, 4H; tpy), 7.76 (s, 2H; tpy), 7.69 (t, $J = 5.7$ Hz, 2H; tpy), 7.49–7.28 (m, 5H; C_6H_5), 4.06 ppm (s, 3H; OCH_3); IR (Nujol): $\tilde{\nu} =$ 3450(br) ν(O-H), 2122(m) ν(C≡C), 1147(m) cm^{-1} ν(S=O); positive-ion FAB-MS: *m*/*z*: 559 $[M-\text{OTf}]^+$; elemental analysis calcd (%) for $C_{25}H_{18}N_3F_3O_4SPt\cdot 0.5H_2O$: C 41.84, H 2.66, N 5.86; found: C 41.71, H 2.56, N 5.76.

General procedure for metathesis reactions: The corresponding derivatives of **1**-OTf and **2**-OTf containing different counter anions were prepared by metathesis reaction. A saturated methanolic solution of the respective ammonium or lithium salts of the anion was added to a solution of **1**-OTf (100 mg, 0.16 mmol) or **2**-OTf (100 mg, 0.15 mmol) in a minimum amount of methanol. The product was isolated by filtration, washed with methanol, and dried. Subsequent recrystallization of the complexes was performed by diffusion of diethyl ether vapor into an acetonitrile solution of the metathesized products.

[Pt(tpy)(C≡C−C≡CH)]PF$_6$ (1-PF$_6$): Yield: 60.7 mg (61%). ^{1}H NMR (300 MHz, CD_3CN, 298 K): $\delta = 8.87$ (d, $J = 5.4$ Hz, 2H; tpy), 8.42 (t, $J =$ 8.1 Hz, 1H; tpy), 8.33–8.22 (m, 6H; tpy), 7.71 (dt, $J = 1.5$, 5.5 Hz, 2H; tpy), 2.26 ppm (s, 1H; acetylenic H); IR (Nujol): $\tilde{\nu} = 3455$(br) ν(O-H), 2159(m), 2012(w) ν(C≡C), 840(s) cm^{-1} ν(P-F); positive-ion FAB-MS: *m*/*z*: 477 $[M-\text{PF}_6]^+$; elemental analysis calcd (%) for $C_{19}H_{12}F_6N_3PPt\cdot 1.5H_2O$: C 35.14, H 2.22, N 6.47; found: C 35.08, H 1.92, N 6.62.

[Pt(tpy)(C≡C−C≡CH)]ClO$_4$ (1-ClO$_4$): Yield: 76.6 mg (83%). ^{1}H NMR (400 MHz, CD_3CN, 298 K): $\delta = 8.99$ (d, $J = 5.0$ Hz, 2H; tpy), 8.43 (t, $J =$ 8.1 Hz, 1H; tpy), 8.36–8.25 (m, 6H; tpy), 7.76 (dt, $J = 1.5$, 5.6 Hz, 2H; tpy), 2.24 ppm (s, 1H; acetylenic H); IR (Nujol): $\tilde{\nu} = 3470$(br) ν(O-H), 2158(m), 2012(w) ν(C≡C), 1097(s) cm^{-1} ν(Cl-O); positive-ion FAB-MS: *m*/*z*: 477 $[M-\text{ClO}_4]^+$; elemental analysis calcd (%) for $C_{19}H_{12}N_3ClO_4Pt\cdot 1.5H_2O$: C 37.79, H 2.50, N 6.96; found: C 37.50, H 2.19, N 6.96.

[Pt(tpy)(C≡C−C≡CH)]BF$_4$ (1-BF$_4$): Yield: 76.7 mg (85%). ^{1}H NMR (400 MHz, CD_3CN, 298 K): $\delta = 9.01$ (d, $J = 5.3$ Hz, 2H; tpy), 8.44 (t, $J =$ 8.2 Hz, 1H; tpy), 8.38–8.26 (m, 6H; tpy), 7.77 (dt, $J = 1.5$, 5.6 Hz, 2H; tpy), 2.24 ppm (s, 1H; acetylenic H); IR (Nujol): $\tilde{\nu} = 3485$(br) ν(O-H), 2158(m), 2012(w) ν(C≡C), 1046(s) cm^{-1} ν(B-F); positive-ion FAB-MS: *m*/*z*: 477 $[M-\text{BF}_4]^+$; elemental analysis calcd (%) for $C_{19}H_{12}F_4N_3BPt\cdot 2H_2O$: C 38.02, H 2.69, N 7.00; found: C 37.87, H 2.30, N 6.98.

[Pt(tpy)(C≡C−C≡CH)]BPh$_4$ (1-BPh$_4$): Yield: 99.3 mg (78%). ^{1}H NMR (400 MHz, CD_3CN, 298 K): $\delta = 8.95$ (d, $J = 5.4$ Hz, 2H; tpy), 8.45 (t, $J =$ 8.1 Hz, 1H; tpy), 8.40–8.25 (m, 6H; tpy), 7.76 (dt, $J = 1.5$, 5.8 Hz, 2H; tpy), 2.29 ppm (s, 1H; acetylenic H); IR (Nujol): $\tilde{\nu} = 2156$(m), 2010(w) cm^{-1} ν(C≡C); positive-ion FAB-MS: *m*/*z*: 477 $[M-\text{BPh}_4]^+$; elemental analysis calcd (%) for $C_{43}H_{32}N_3BPt$: C 64.83, H 4.05, N 5.27; found: C 64.63, H 3.95, N 5.54.

[Pt(tpy)(C≡CC$_6$H$_5$)]PF$_6$ (2-PF$_6$): Yield: 60.7 mg (60%). ^{1}H NMR (300 MHz, CD_3CN, 298 K): $\delta = 8.67$ (d, $J = 6.1$ Hz, 2H; tpy), 8.25–8.02 (m, 7H; tpy), 7.55 (t, $J = 6.5$ Hz, 2H; tpy), 7.43–7.19 ppm (m, 5H; C_6H_5); IR (Nujol): $\tilde{\nu} = 2126$(m) ν(C≡C), 841(s) cm^{-1} ν(P-F); positive-ion FAB-MS: *m*/*z*: 529 $[M-\text{PF}_6]^+$; elemental analysis calcd (%) for $C_{23}H_{16}F_6N_3PPt$: C 40.90, H 2.37, N 6.23; found: C 40.87, H 2.36, N 6.23.

[Pt(tpy)(C≡CC$_6$H$_5$)]ClO$_4$ (2-ClO$_4$): Yield: 62.2 mg (66%). ^{1}H NMR (300 MHz, CD_3CN, 298 K): $\delta = 9.16$ (d, $J = 6.2$ Hz, 2H; tpy), 8.41–8.17 (m, 7H; tpy), 7.75 (t, $J = 6.5$ Hz, 2H; tpy), 7.51–7.30 ppm (m, 5H; C_6H_5); IR (Nujol): $\tilde{\nu} = 2122$(m) ν(C≡C), 1095(s) cm^{-1} ν(Cl-O); positive-ion FAB-MS: *m*/*z*: 529 $[M-\text{ClO}_4]^+$; elemental analysis calcd (%) for $C_{23}H_{16}ClN_3O_4Pt$: C 43.92, H 2.56, N 6.68; found: C 43.69, H 2.62, N 6.35.

[Pt(tpy)(C≡CC$_6$H$_5$)]BF$_4$ (2-BF$_4$): Yield: 69.3 mg (75%). ^{1}H NMR (300 MHz, CD_3CN, 298 K): $\delta = 9.02$ (d, $J = 6.3$ Hz, 2H; tpy), 8.35–8.12 (m, 7H; tpy), 7.69 (t, $J = 6.0$ Hz, 2H; tpy), 7.45–7.29 ppm (m, 5H; C_6H_5); IR (Nujol): $\tilde{\nu} = 3450$(br) ν(O-H), 2122(m) ν(C≡C), 1056(s) cm^{-1} ν(B-F); positive-ion FAB-MS: *m*/*z*: 529 $[M-\text{BF}_4]^+$; elemental analysis calcd (%) for $C_{23}H_{16}F_4N_3BPt\cdot 0.5H_2O$: C 44.18, H 2.74, N 6.72; found: C 44.30, H 2.74, N 6.72.

Acknowledgements

V. W.-W. Y. acknowledges support from the University Development Fund of The University of Hong Kong and The University of Hong Kong Foundation for Educational Development and Research Limited. The work described in this paper has been supported by a CERG Grant from the Research Grants Council of Hong Kong Special Administrative Region, China (Project No. HKU 7022/03P). K. H.-Y. C. acknowledges the receipt of a postgraduate studentship, administered by The University of Hong Kong.

[1] a) J. W. Schindler, R. C. Fukuda, A. W. Adamson, *J. Am. Chem. Soc.* **1982**, *104*, 3596–3600; b) J. Biedermann, G. Gliemann, U. Klement, K. J. Range, M. Zabel, *Inorg. Chem.* **1990**, *29*, 1884–1888; c) V. M. Miskowski, V. H. Houlding, C. M. Che, Y. Wang, *Inorg. Chem.* **1993**, *32*, 2518–2524; d) C. A. Daws, C. L. Exstrom, J. R. Sowa, Jr., K. R. Mann, *Chem. Mater.* **1997**, *9*, 363–368; e) H. Yersin, W. Humbs, J. Strasser, *Coord. Chem. Rev.* **1997**, *159*, 325–358; f) H. K. Yip, H. M. Lin, Y. Wang, C. M. Che, *Inorg. Chem.* **1993**, *32*, 3402–3407; g) V. Adamovich, J. Brooks, A. Tamayo, A. M. Alexander, P. I. Djurovich,

B. W. D'Andrade, C. Adachi, S. R. Forrest, M. E. Thompson, *New J. Chem.* **2002**, *26*, 1171–1178.

[2] a) D. M. Roundhill, H. B. Gray, C. M. Che, *Acc. Chem. Res.* **1989**, *22*, 55–61; b) V. M. Miskowski, V. H. Houlding, *Inorg. Chem.* **1989**, *28*, 1529–1533; c) V. M. Miskowski, V. H. Houlding, *Inorg. Chem.* **1991**, *30*, 4446–4452; d) J. J. Novoa, G. Aullón, P. Alemany, S. Alvarez, *J. Am. Chem. Soc.* **1995**, *117*, 7169–7171; e) B. Ma, J. Li, P. I. Djurovich, M. Yousufuddin, R. Bau, M. E. Thompson, *J. Am. Chem. Soc.* **2005**, *127*, 28–29.

[3] a) K. W. Jennette, J. T. Gill, J. A. Sadownick, S. J. Lippard, *J. Am. Chem. Soc.* **1976**, *98*, 6159–6168; b) B. C. Tzeng, W. F. Fu, C. M. Che, H. Y. Chao, K. K. Cheung, S. M. Peng, *J. Chem. Soc. Dalton Trans.* **1999**, 1017–1023; c) H. K. Yip, C. M. Che, Z. Y. Zhou, T. C. W. Mak, *J. Chem. Soc. Chem. Commun.* **1992**, 1369–1371; d) H. K. Yip, L. K. Cheng, K. K. Cheung, C. M. Che, *J. Chem. Soc. Dalton Trans.* **1993**, 2933–2938; e) W. Lu, M. C. W. Chan, N. Zhu, C. M. Che, C. Li, Z. Hui, *J. Am. Chem. Soc.* **2004**, *126*, 7639–7651; f) J. A. Bally, V. M. Miskowski, H. B. Gray, *Inorg. Chem.* **1993**, *32*, 369–370; g) C. Yu, K. M. C. Wong, K. H. Y. Chan, V. W. W. Yam, *Angew. Chem.* **2005**, *117*, 801–804; *Angew. Chem. Int. Ed.* **2005**, *44*, 791–794.

[4] V. W. W. Yam, K. M. C. Wong, N. Zhu, *J. Am. Chem. Soc.* **2002**, *124*, 6506–6507.

[5] a) V. W. W. Yam, R. P. L. Tang, K. M. C. Wong, K. K. Cheung, *Organometallics* **2001**, *20*, 4476–4482; b) V. W. W. Yam, R. P. L. Tang, K. M. C. Wong, X. X. Lu, K. K. Cheung, N. Zhu, *Chem. Eur. J.* **2002**, *8*, 4066–4076; c) V. W. W. Yam, K. M. C. Wong, N. Zhu, *Angew. Chem.* **2003**, *115*, 1438–1441; *Angew. Chem. Int. Ed.* **2003**, *42*, 1400–1403; d) K. M. C. Wong, W. S. Tang, B. W. K. Chu, N. Zhu, V. W. W. Yam, *Organometallics* **2004**, *23*, 3459–3465.

[6] a) T. K. Aldridge, E. M. Stacy, D. R. McMillin, *Inorg. Chem.* **1994**, *33*, 722–727; b) S. W. Lai, M. C. W. Chan, K. K. Cheung, C. M. Che, *Inorg. Chem.* **1999**, *38*, 4262–4267; c) J. F. Michalec, S. A. Bejune, D. R. McMillin, *Inorg. Chem.* **2000**, *39*, 2708–2709; d) D. K. Crites, C. T. Cunningham, D. R. McMillin, *Inorg. Chim. Acta* **1998**, *273*, 346–353; e) D. R. McMillin, J. J. Moore, *Coord. Chem. Rev.* **2002**, *229*, 113–121.

[7] a) J. A. Bailey, M. G. Hill, R. E. Marsh, V. M. Miskowski, W. P. Schaefer, H. B. Gray, *Inorg. Chem.* **1995**, *34*, 4591–4599; b) R. Büchner, J. S. Field, R. J. Haines, C. T. Cunningham, D. R. McMillin, *Inorg. Chem.* **1997**, *36*, 3952–3956; c) R. Büchner, C. T. Cunningham, J. S. Field, R. J. Haines, D. R. McMillin, G. C. Summerton, *J. Chem. Soc. Dalton Trans.* **1999**, 711–718; d) T. J. Wadas, Q. M. Wang, Y. J. Kim, C. Flaschenreim, T. N. Blanton, R. Eisenberg, *J. Am. Chem. Soc.* **2004**, *126*, 16841–16849.

[8] a) R. S. Osborn, D. Rogers, *J. Chem. Soc. Dalton Trans.* **1974**, 1002–1004; b) W. B. Connick, R. E. Marsh, W. P. Schaefer, H. B. Gray, *Inorg. Chem.* **1997**, *36*, 913–922; c) R. H. Herber, M. Croft, M. J. Coyer, B. Bilash, A. Sahiner, *Inorg. Chem.* **1994**, *33*, 2422–2426; d) W. B. Connick, L. M. Henling, R. E. Marsh, H. B. Gray, *Inorg. Chem.* **1996**, *35*, 6261–6265.

[9] a) S. A. C. McDowell, *Phys. Chem. Chem. Phys.* **2001**, *3*, 2754–2757; b) E. J. L. McInnes, A. J. Welch, L. J. Yellowlees, *Acta Cryst.* **1995**, *C51*, 2023–2025; c) D. Braga, F. Grepioni, E. Tedesco, M. J. Calhorda, P. E. M. Lopes, *New J. Chem.* **1999**, *23*, 219–226.

[10] a) J. N. Demas, G. A. Crosby, *J. Phys. Chem.* **1971**, *75*, 991–1024; b) J. Van Houten, R. J. Watts, *J. Am. Chem. Soc.* **1976**, *98*, 4853–4858; c) L. Wallace, D. P. Rillema, *Inorg. Chem.* **1993**, *32*, 3836–3843.

[11] a) Z. Otwinowski, W. Minor, "Processing of X-ray Diffraction Data Collected in Oscillation Mode" in *Methods in Enzymology, Vol. 276: Macromolecular Crystallography, Part A* (Eds.: C. W. Carter, R. M. Sweet, Jr.), Academic Press, **1997**, pp. 307–326; b) G. M. Sheldrick, SHELXS-97, Programs for Crystal Structure Analysis (Release 97–2), University of Göttingen, Göttingen (Germany), **1997**; c) G. M. Sheldrick, SHELXL-97, Programs for Crystal Structure Analysis (Release 97–2), University of Göttingen, Göttingen, (Germany), **1997**; d) $R_{int} = \Sigma |F_o^2 - F_o^2(\text{mean})| / \Sigma [F_o^2]$.

Received: January 29, 2005
Published online: June 18, 2005

